RESONANT BEHAVIOR MEASUREMENTS AND TWO-DIMENSIONAL IMAGING OF SMALL CONDUCTING SPHERES IN CATR

S. H. Quan and Q. H. Liu

Beijing University of Aeronautics and Astronautics (BUAA)
Beijing 100191, China

Abstract—Based on swept frequency RCS measurement system, low density foam column and proper data processing procedure, the resonance curves of conducting spheres with RCS below -32.95 dBsm are achieved in a single reflector Compact Antenna Test Range (CATR), with the measurement errors less than 1.0 dB over most of the measurement frequencies. Nine spheres down to -49.01 dBsm are clearly imaged with Range-Doppler (R-D) method and pointwise vector background subtraction technique.

1. INTRODUCTION

With the development of stealth technology, the power that a radar can receive from a stealth target is decreasing. As a result, RCS (radar cross section) measurements, especially accurate and indoor RCS measurements have become increasingly important for military applications. Therefore, it is useful to study low RCS measurements and error correction techniques in CATR (compact antenna test range).

There are various factors that affect RCS measurement accuracy in CATR, including selection of the support, setting of the test system, and data processing procedure such as gate function in the time domain and window function in the frequency domain, etc. [1–6].

There are mainly three practical ways to support the test target: low density foam column, low-scattering metal pylon and string suspension system [7, 8]. The limitation of the string suspension system in attitude control makes it scarcely to be adopted in imaging. The low-scattering metal pylon has the problem of coupling with the test target, though the great strength and excellent characteristics at high

---

Corresponding author: S. H. Quan (eie205@hotmail.com).

frequency make it very useful. The low density foam column can overcome these problems when the target is light and the frequency is below Ka band.

However, when a stepped frequency rotation measurement is performed, the foam column will rotate with the target. A certain orientation of the foam column is measured mostly to serve as the background, which will be time-saving but bring target measurement errors caused by the inhomogeneity of the foam.

In order to isolate system coupling, reflector reflection, and sidelobe leakage from the feed, gate function is applied to the time domain. In order to suppress the sidelobes, window function in the frequency domain is chosen.

To the interest of weighing the accuracy of the measurements, conducting spheres are always selected, whose analytical solution exists [9, 10].

The resonance curve of a 40.0 cm conducting sphere is successfully achieved by the UAV Specialty Technique Key Laboratory of National Defense Technology in Northwestern Polytechnic University [11], and the measurement errors are within 1.0 dB in X-band. Marion Baggett has measured the RCS of a 35.56 cm conducting sphere between 2.0 GHz and 36.0 GHz, whose error is below 2.0 dB in the whole band [12].

In this paper, the resonance curves of small conducting spheres below -32.95 dBsm are successfully achieved, and nine spheres as low as -49.01 dBsm are clearly imaged with Range-Doppler (R-D) method [13, 14]. A network analyzer and a low density foam column are used. The pointwise vector background subtraction technique is applied to ensure that the measurement errors are within 1.0 dB over most of the measurement frequencies.

2. SYSTEM COMPOSITION AND MEASUREMENT METHOD

The RCS measurement system can be divided into single frequency system and swept frequency system. Considering the performance and accuracy, the swept frequency system is more widely used [4, 5]. The Agilent E8363B vector network analyzer is selected. The measurement system and methods are as follows.

2.1. Swept Frequency RCS Measurement System Composition

The swept frequency RCS measurement system is mainly composed of CATR antenna system, supporting system, vector network analyzer and control system. The system diagram is shown in Fig. 1, and the target to be measured is placed in the quiet zone. The quiet zone is 2.0 m in diameter and has ± 0.2 dB amplitude ripple, 0.7 dB amplitude taper and 5.0 degree phase variation over the measurement frequencies.

2.2. Swept Frequency RCS Measurement Method

We can heighten the system power or reduce the IF band to suppress the system noise and improve the test accuracy.

Taking the test time and power limitation of the system into account, we set the power at 0.0 dBm and IF bandwidth at 50.0 Hz.

The swept frequency RCS measurement program can be divided into the following steps: swept measurements, background subtraction, inverse windowed Fourier transform, rectangular gate filtering, Fourier transform to the frequency domain and calibration. Fig. 2 specifies the procedure mentioned above, in which the choice of window function and width of gate function are two important steps for data processing.
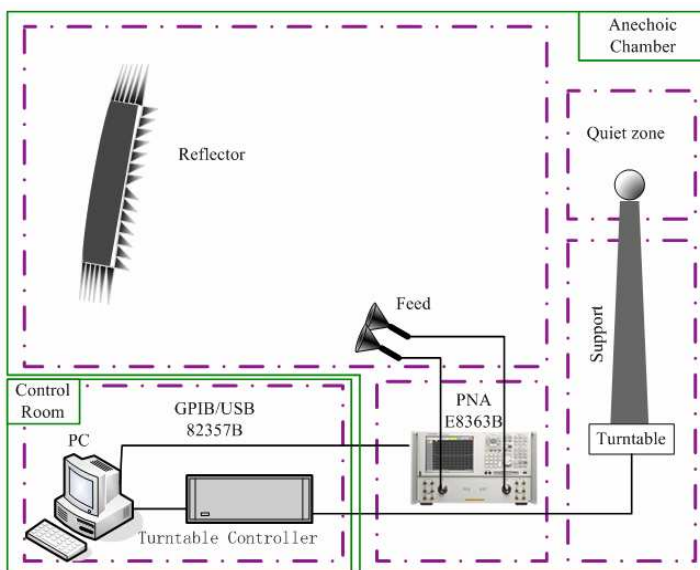

Figure 1. Measurement system.

We select Kaiser Window as the window function in this experiment, as shown in formula (1).

$$W(k) = \frac{I_0\left[\beta\sqrt{1 - \left(1 - \frac{2k}{N-1}\right)^2}\right]}{I_0(\beta)} \quad 0 \leq k \leq N - 1, \quad (1)$$

where, $I_0(\beta)$ is the zeroth order modified Bessel function of the first kind, and β is an arbitrary real number that determines the shape of the window. We set $\beta = 5.6$ here.

In addition, the width of the gate function is also important for the accuracy. We should retain as many details of the target signal as possible, and avoid unwanted signals falling into the gate function. Here, the width is 2.0 m.

In order to analyze scattering characteristics of different parts of the target, two-dimensional imaging approach is applied. As the support has a great impact on the test results in low RCS measurements, the rotation vector background subtraction technique is used. The steps are as follows.

(1) A stepped frequency rotation is performed on the test target and foam together;

(2) A stepped frequency rotation is performed on the foam column alone.

(3) The stepped frequency calibration data is collected at a fixed position.

(4) Following the steps in Fig. 2, the target RCS in the frequency domain is obtained;
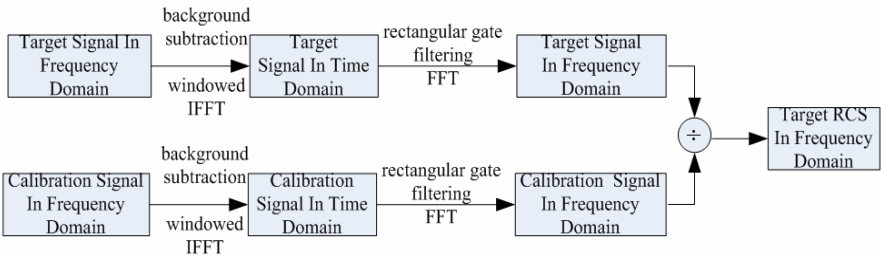
(5) Two-dimensional Imaging with R-D method.

Figure 2. Processes of swept frequency RCS measurements.

3. TEST TARGETS AND SUPPORT CONFIGURATION

RCS of electrically large and complex targets is difficult or impossible to be obtained with the analytical method, and it will take a long time to achieve the RCS with the methods of moment (MOM), finite element (FEM) or finite-difference time-domain method (FDTD), etc. [15–18], which makes the measurement more important.

In order to weigh the accuracy of the measurement, we select conducting spheres as the test targets, whose analytical solution exists.

According to the ratio of the radius of the conducting sphere to the wavelength, the sphere RCS is divided into three regions: Rayleigh zone, resonance zone and optical zone, where the RCS is approximately πa^2 in optical zone. Characteristics of the conducting spheres under test are shown in Table 1.

These spheres are mostly within the resonance region in X band (8.0 GHz–12.0 GHz). So the theoretical value will fluctuate around πa^2. Resonance curves of these spheres will be measured in the following section.

Considering the measured frequency and target characteristics, we select a kind of foam column as shown in Fig. 3, whose top and bottom diameters are about 20.0 cm and 40.0 cm respectively. A short foam column with 60.0 cm diameter is also selected to place these spheres.
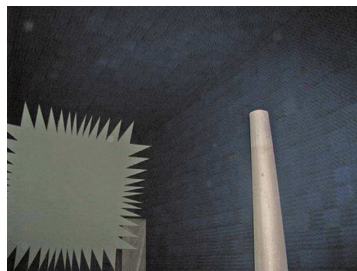

Figure 3. Support and measurement environment.

Table 1. Conducting spheres and their RCS.

No.	1	2	3	4	5
radius (mm)	12.71	11.15	5	4	3.5
RCS (dBsm)	−32.95	−34.08	−41.05	−42.99	−44.15
No.	6	7	8	9	
radius (mm)	3.16	3	2.5	2	
RCS (dBsm)	−45.03	−45.49	−47.07	−49.01	

4. EXPERIMENTAL RESULTS

4.1. Resonance Curve Measurements of Conducting Spheres

The exact solution for the scattering of a perfectly conducting sphere
is known as the Mie series [19–22], which can be expressed as

$$\sigma = \frac{\lambda^2}{\pi} \left| \sum_{n=1}^{\infty} (-1)^n (n + 0.5) (b_n - a_n) \right|^2, \tag{2}$$

where

$$a_n = \frac{j_n(ka)}{h_n^{(1)}(ka)} \tag{3}$$

and

$$b_n = \frac{ka j_{n-1}(ka) - n j_n(ka)}{ka h_{n-1}^{(1)}(ka) - n h_n^{(1)}(ka)}, \tag{4}$$

where a is the sphere radius; λ is the wavelength; $k = 2\pi/\lambda$ is the wave
number; $j_n(x)$ is the spherical Bessel function of the first kind; $h_n^{(1)}(x)$
is the spherical Hankel function of the first kind. The normalized RCS
is as follows.

$$\sigma_{\text{normal}} = \frac{\sigma}{\pi a^2} = \left(\frac{2}{ka} \right)^2 \left| \sum_{n=1}^{\infty} (-1)^n (n + 0.5) (b_n - a_n) \right|^2 \tag{5}$$
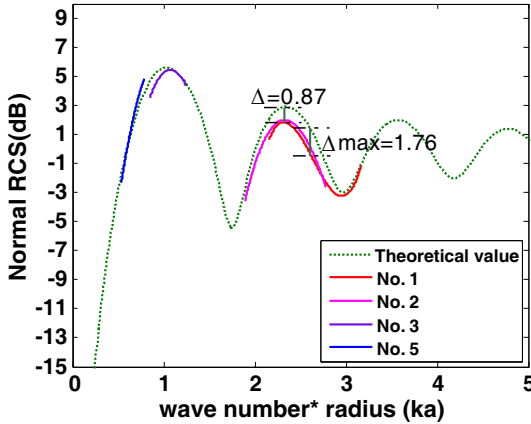

Figure 4. The comparison between the theoretical normalized RCS
and the measured normalized RCS.

We select No. 1, No. 2, No. 3 and No. 5 as examples. Fig. 4 is the comparison between the theoretical normalized RCS curve and measured normalized RCS curves, where the horizontal axis is the product of the wave number and the sphere radius, and the vertical axis is the normalized RCS.

It can be seen that with appropriate measurement programs and suitable data processing methods, we can achieve a RCS down to −44.15 dBsm and ensure that the measurement errors are mostly within 1.0 dB, while the maximum may reach 1.76 dB in certain frequencies.

4.2. Pointwise Vector Background Subtraction Imaging

Two-dimensional imaging is an important way to detect the distribution of the target scattering centers, which are of great importance for the stealth structure design.

However, in low RCS measurement process, the support itself has an additional RCS, which will result in testing errors, unclear images or abnormal scattering centers.

So rotation pointwise vector background subtraction technique and R-D imaging method are employed. In the imaging process, the selected step angle is 0.25 degree, and the angle range is 30.0 degrees. Fig. 5 shows the position of the nine spheres.

Figures 6 to 8 show the images of the support itself, the target with a single point vector background subtraction and the target with the rotation pointwise vector background subtraction.

It can be seen that the support RCS is around −45.0 dBsm,
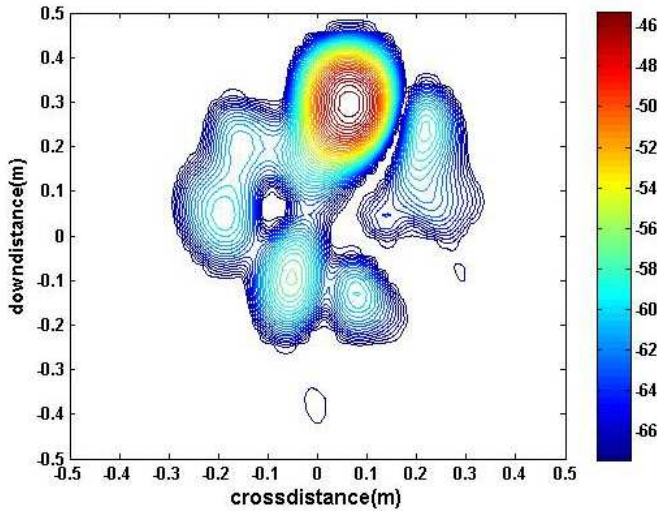

Figure 5. The position of the nine spheres.
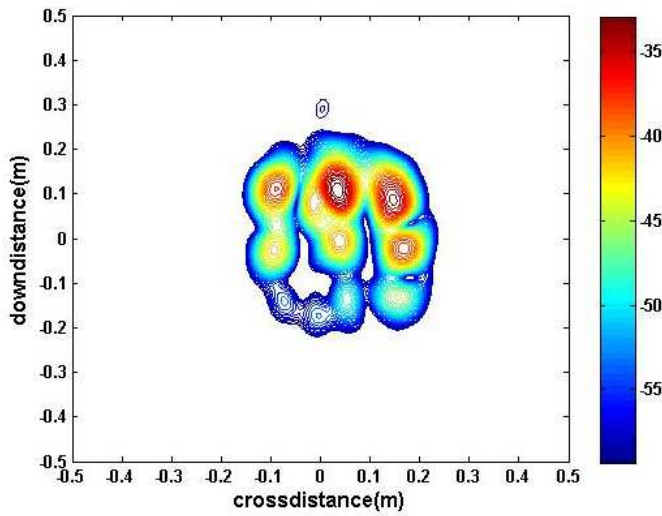
Figure 6. Foam column image.

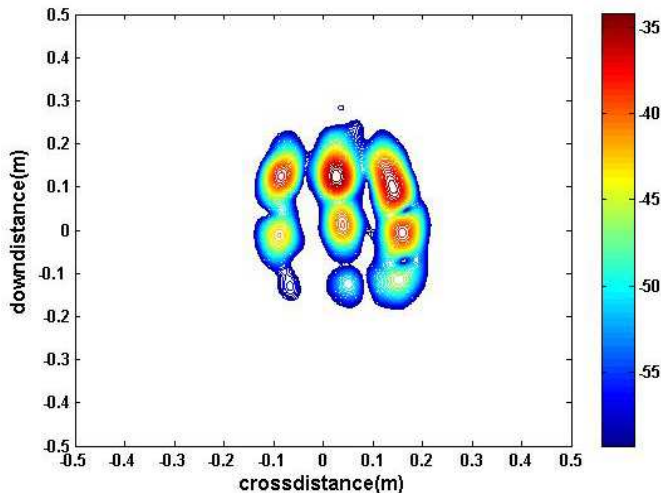**Figure 7.** Target image with a single point background subtraction.

Figure 8. Target image with pointwise vector background subtraction.

and there will be some abnormal scattering centers between No. 2 and No. 3, No. 8 and No. 9 using a single point vector background subtraction. While by the pointwise vector background subtraction, only the spheres are clearly shown, and the clutters are effectively suppressed.

When the target RCS is much higher than the support itself, the imaging result with a single point subtraction is basically the same as that of the pointwise subtraction. However, the latter will consume more time. In addition, the long-term test may also result in system drifting, which will lead to the background subtraction deterioration, or even produce exactly the opposite results.

Generally, the pointwise vector background subtraction technique is more effective for low RCS target measurements and short time tests.

5. CONCLUSION

In this paper, the resonance curves of different small conducting spheres have been achieved, with the measurement errors within $1.0 \, \mathrm{dB}$ over most of the measurement frequencies. Then, by employing the pointwise vector background subtraction technique and R-D imaging method in two-dimensional imaging, we finally succeeded in obtaining the images of nine conducting spheres with RCS down to $-49.01 \, \mathrm{dBsm}$.

ACKNOWLEDGMENT

REFERENCES

1. Knott, E. F., *Radar Cross Section Measurements*, Van Nostrand Reinhold, New York, 2006.

2. Kent, B. M., "Comparative measurements of precision radar cross section (RCS) calibration targets," *IEEE Antennas and Propagation Society International Symposium*, Vol. 4, 412–415, 2001.

3. Li, Y.-L., et al., "Scattering field for the ellipsoidal targets irradiated by an electromagnetic wave with arbitrary polarizing and propagating direction," *Progress In Electromagnetics Research Letters*, Vol. 1, 221–235, 2008.

4. Miacci, M. A. S., I. M. Martin, and M. C. Rezende, "Radar cross section measurements of complex targets (missile parts) in C-band in anechoic chamber," *Microwave and Optoelectronics Conference*, 401–405, Nov. 2007.

5. Hess, D. W., "Introduction to RCS measurements," *Antennas and Propagation Conference*, 37–44, Mar. 2008.

6. Lorant, A. M., C. M. Wang, and T. Conn, "Robust separation of background and target signals in radar cross section measurements," *IEEE Transactions on Instrumentation and Measurement*, Vol. 54, No. 6, 2462–2468, Dec. 2005.

7. Jeffery, A. B. and G. L. Wilson, "Design of target support columns using EPS foam," *IEEE Antennas and Propagation Magazine*, Vol. 45, No. 1, Feb. 2003.

8. Burns, J. W., E. I. Lebaron, and G. G. Fliss, "Characterization of target-pylon interactions in RCS measurements," *Antennas and Propagation Society International Symposium*, Vol. 1, 13–18, Jul. 1997.

9. Hamid, A. K. and M. Hamid, "Electromagnetic scattering by an array of conducting spheres each coated with a dielectric layer," *Antennas and Propagation Society International Symposium*, Vol. 1, 8–13, Jul. 2001.

10. Hamid, A. K., I. R. Ciric, and M. Hamid, "Analytic solution of scattering by an array of conducting spheres," *Antennas*

      and Propagation Society International Symposium, Vol. 3, 7–11,
      May 1990.

11.   Hu, C.-F., J.-D. Xu, N. J. Li, and L.-X. Zhang, "Indoor
      accurate RCS measurement technique on UHF band," *Progress
      In Electromagnetics Research*, PIER 81, 279–289, 2008.

12.   Baggett, M. and T. Thomas, "Obtaining high quality RCS
      measurements with a very large foam column," *AMTA Symposium
      Digest*, 2005.

13.   Ausherman, D. A., A. Kozma, J. L. Walker, H. M. Jones,
      and E. C. Poggio, "Developments in radar imaging," *IEEE
      Transactions on Aerospace and Electronic Systems*, Vol. 20, No. 4,
      363–400, Jul. 1984.

14.   Mensa, D. L., *High Resolution Radar Cross-section Imaging*,
      Artech House, Inc., 1990.

15.   Li, B. K., F. Liu, and S. Crozier, "High-field magnetic resonance
      imaging with reduced field/tissue RF artefacts — A modeling
      study using hybrid MoM/FEM and FDTD technique," *IEEE
      Transactions on Electromagnetic Compatibility*, Vol. 48, No. 4,
      Nov. 1993.

16.   Hatamzadeh-Varmazyar, S., M. Naser-Moghadasi, and Z. Ma-
      souri, "A moment method simulation of electromagnetic scatter-
      ing from conducting bodies," *Progress In Electromagnetics Re-
      search*, PIER 81, 99–119, 2008.

17.   Wang, S., X. Guan, D.Wang, X. Ma, and Y. Su, "Electromagnetic
      scattering by mixed conducting/dielectric objects using higher
      order MoM," *Progress In Electromagnetics Research*, PIER 66,
      51–63, 2006.

18.   Hu, B., X.-W. Xu, M. He, and Y. Zheng, "More accurate
      hybrid PO-MoM analysis for an electrically large antenna-radome
      structure," *Progress In Electromagnetics Research*, PIER 92, 255–
      265, 2009.

19.   Bowman, J. J., et al., *Electromagnetic and Acoustic Scattering by
      Simple Shapes*, North-Holland Publishing, Amsterdam, 1969.

20.   Li, Z., et al., *Commonly used Method in Radar Cross Section
      Calculation*, Institute of Target Characteristics, Beijing, 1981.

21.   Rother, T. and K. Schmidt, "The discretized Mie-formalism
      for electromagnetic scattering," *Progress In Electromagnetics
      Research*, PIER 17, 91–183, 1997.

22.   Censor, D., "Non-relativistic scattering in the presence of moving
      objects: The Mie problem for a moving sphere," *Progress In
      Electromagnetics Research*, PIER 46, 1–32, 2004.